Cancer Immunol Immunother (2010) 59:149–159
DOI 10.1007/s00262-009-0735-2

ORIGINAL ARTICLE

Calicum microdomains form within neutrophils at the neutrophil–tumor cell synapse: role in antibody-dependent target cell apoptosis

Andrea J. Clark · Michelle Diamond · Megan Elfline · Howard R. Petty

Received: 6 May 2009 / Accepted: 29 June 2009 / Published online: 11 July 2009

Abstract Ca^{2+} messages are broadly important in cellular signal transduction. In immune cells, Ca^{2+} signaling is an essential step in many forms of activation. Neutrophil-mediated antibody-dependent cell-mediated cytotoxicity (ADCC) is one form of leukocyte activation that plays an important role in tumor cell killing in vitro and in patient care. Using fluorescence methodologies, we found that neutrophils exhibit Ca^{2+} signals during ADCC directed against breast fibrosarcoma cells. Importantly, these signals were localized to Ca^{2+} microdomains at the neutrophil-to-tumor cell interface where they display dynamic features such as movement, fusion, and fission. These signals were blocked by the intracellular Ca^{2+} buffer BAPTA. At the neutrophil–tumor cell synapse, the neutrophil's cytoplasm was enriched in STIM1, a crucial mediator of Ca^{2+} signaling, whereas the Ca^{2+}-binding proteins calbindin and parvalbumin were not affected. Our findings suggest that Ca^{2+} microdomains are due to an active signaling process. As Ca^{2+} signals within neutrophils were necessary for specific tumor cell apoptosis, a central role of microdomains in leukocyte-mediated tumor cell destruction is indicated.

Keywords Breast cancer · Apoptosis · Antibody · Signal transduction · Calcium

Introduction

Anti-tumor antibodies (Abs) represent a targeted immunotherapeutic approach that holds great promise in patient care. Indeed, nine mAbs including Herceptin, Erbitux, Rituxan and Avastin have received FDA approval and are used clinically [1, 2]. Some of these biopharmaceuticals, such as Bexxar, are immunoconjugates that deliver a radiolabel or cytotoxin directly to a target cell. Others may block cell surface growth factor receptors that promote cell proliferation. A major contributor to the efficacy of mAb therapy is their ability to stimulate Ab-dependent cell-mediated cytotoxicity (ADCC) [1, 3, 4]. ADCC is the attack of immune effector cells bearing receptors for Ab molecules (FcR) upon Ab-coated tumor cells. Early in vivo studies demonstrated the efficacy of Ab therapy in murine models of metastasis [5, 6]. Using Fc$R\gamma^{-/-}$ mice, Clynes et al. [7] demonstrated that FcRs were necessary for passive and active Ab-dependent immunity in a melanoma model. Subsequently, Clynes et al. [8] demonstrated that Ab-dependent anti-tumor immunity is considerably enhanced in knock-out mice lacking the inhibitory FcγRIIB molecule. The role of FcRs in Ab-based human therapies finds support in recent clinical studies showing that FcγR polymorphisms correlate with the efficacy of mAb therapy [e.g., 9–11]. ADCC has been demonstrated for FcR-positive cells including macrophage/monocytes, neutrophils, and NK cells [3, 12]. Recently, interest in neutrophil-mediated ADCC has increased because it participates in anti-tumor responses to a broad range of malignancies in vitro [12–16] and is likely to be a key contributor to mAb therapy in patients [1, 3].

Electronic supplementary material The online version of this article (doi:10.1007/s00262-009-0735-2) contains supplementary material, which is available to authorized users.

A. J. Clark · M. Diamond · M. Elfline · H. R. Petty (✉)
Department of Ophthalmology and Visual Sciences,
The University of Michigan Medical School,
1000 Wall Street, Ann Arbor, MI 48105, USA
e-mail: hpetty@umich.edu

H. R. Petty
Department of Microbiology and Immunology,
The University of Michigan Medical School,
Ann Arbor, MI 48105, USA

Although proteins participating in FcγR activation (e.g., FcγRIII, FcγRIIA, Syk, PLCγ, and $InsP_3R$) as well as their covalent modifications (phosphorylation and palmitoylation) have been described [e.g., 17], the actions of these proteins have not been integrated with downstream Ca^{2+}-signaling events [8, 12]. Moreover, the spatio-temporal dynamics of associated Ca^{2+} signals are unknown. In contrast to previous work suggesting that Ca^{2+} signals are distributed throughout immune cells, we have discovered that Ca^{2+} signals are in the form of microdomains at the neutrophil–tumor cell synapse. These microdomains likely direct leukocyte effector functions toward the target cell, including leukocyte-mediated activation of a tumor cell's apoptotic signaling pathways. Indeed, leukocyte Ca^{2+} microdomains may be a general feature of cell-mediated tumor cell attack.

Materials and methods

Materials

Fura red-acetoxymethyl ester (Fura red-AM), fluo-4-acetoxymethyl ester (Fluo-4-AM), BAPTA-AM (1,2-bis (2-aminophenoxy)-*N*,*N*,*N*′,*N*′-tetraacetic acid tetra(acetoxymethyl)ester), pluronic-127, cell culture media, and phosphate-buffered saline (PBS) were obtained from Invitrogen Corp. (Carlsbad, CA). NucView™ 488 caspase-3 assay kit was obtained from Biotium Inc. (Hayward, CA). Cover-glass bottom dishes were purchased from MatTek Corporation (Ashland, MA). Unless otherwise noted, chemicals were obtained from Sigma Chemical Company (St. Louis, MO).

Neutrophil preparation

Peripheral blood was collected from healthy human donors in compliance with the guidelines of the University of Michigan Institutional Review Board for Human Subject Research. Neutrophils were isolated using Ficoll-Histopaque (Sigma) density gradient centrifugation, then resuspended and washed in PBS by centrifugation. Adherent HT-1080 cells and neutrophils were co-incubated at an effector-to-target ratio of 50:1, unless otherwise noted.

HT-1080 cell growth and opsonization

The HT-1080 human breast fibrosarcoma cell line (American Type Culture Collection CCL-121, Marassas, VA) was maintained on plastic tissue culture flasks in Dulbecco's modified Eagle medium (DMEM, Invitrogen) containing 10% heat-inactivated FBS (Invitrogen) and 1% antibiotic/antimycotic (Invitrogen). Cells were transferred to fresh media then plated onto glass cover slips or cover-glass bottom dishes 24 h before use. For most experiments, cells on cover slips were opsonized for 30 min with rabbit IgG anti-human β2-microglobulin Ab (Accurate Chemical and Scientific Corp., Westbury, NY) then washed with media. To avoid confounding Ab cross-reactivity, calbindin, parvalbumin, and STIM1 (stromal interaction molecule-1) Ab staining protocols employed HT-1080 cells opsonized with an anti-human β2-microglobulin IgG2a Ab (Santa Cruz Biotechnology, Santa Cruz, CA).

Cell treatments

After a minimum of 24 h of cell growth on cover-glass bottom dishes, tumor cells were opsonized with IgG (experiments) or not (controls). Studies included tumor cell exposure to: nothing, 100 μM hydrogen peroxide, IgG alone, neutrophils without IgG, BAPTA-AM-treated neutrophils with IgG, or untreated neutrophils plus IgG. Cells were co-incubated at 37°C for 1 h in caspase-3 assays, 4 h in GAPDH studies, and 3 h in annexin V studies. In calbindin, parvalbumin, and STIM1 staining experiments, tumor cells were incubated with neutrophils or controls at 37°C for 30 min to 1 h.

Caspase-3 activation assay

Neutrophils were incubated with tumor cells for 30 min at 37°C. NucView™ 488 caspase-3 substrate was added to a final concentration of 5 μM at 37°C. After 30 additional minutes, cells were washed and transferred to a heated fluorescence microscope stage held at 37°C.

Annexin V-binding assay

Neutrophils were incubated with tumor cells for 3 h at 37°C. After the plates were washed, 5 μl of Alexa Fluor 555-conjugated annexin V (Invitrogen) was added to 100 μl of DMEM for each plate and incubated at room temperature for 15 min. In some cases, an Alexa Fluor 350-conjugated annexin V label was employed. The plates were washed again then imaged using fluorescence microscopy.

Immunofluorescence staining

Samples were fixed using a modified version of the dithiobis(succinimidyl propionate) (DSP) procedure [18], which provides superior retention of labile cellular structures. Briefly, cells were first fixed using DSP (1 mg/ml; Pierce, Rockford, IL) in PBS for 15 min at room temperature. Cells were then extracted using 100% ethanol, washed with PBS, fixed with 3.7% paraformaldehyde for 20 min, and then washed with PBS.

Samples were blocked with Image-iT FX (Invitrogen), a signal enhancer, for 30 min before staining, and an

endogenous biotin-blocking kit was used as described by the manufacturer (Invitrogen). The samples were washed then labeled with primary Abs for 1 h. Primary Abs used included anti-glyceraldehyde 3-phosphate dehydrogenase (GAPDH) Ab (Chemicon International), anti-calbindin Ab (Abcam), anti-parvalbumin Ab (Abcam) or anti-STIM1 Ab (ProSci Incorporated). After a thorough wash with PBS, they were incubated for 1 h with biotin-XX-conjugated goat anti-rabbit or goat anti-mouse IgG (Invitrogen). Cells were washed followed by a 30-min treatment with Alexa Fluor 594-conjugated streptavadin (Invitrogen). After streptavadin treatment, cells were washed again with PBS and imaged.

Fluorescence microscopy

Fluorescence microscopy was performed using a 60× oil immersion Plan Apo objective (NA = 1.45) (Nikon, Melville, NY) and an Andor iXon camera (Andor Technology, Belfast, Northern Ireland) attached to the bottom port of a Nikon TE2000-U inverted microscope (Nikon) with a 100-W mercury lamp. Alexa Fluor 594 streptavadin and Alexa Fluor 555 annexin V were imaged using a Nikon 96321 filter set comprised of a 570 nm dichroic mirror, a 530–560 nm excitation filter, and a 590–650 nm emission filter. Serial sections in the *z*-axis of the cells were collected using a Z-drive (Nikon). A QImaging Retiga 1300 camera (QImaging, Surrey, BC) was used to obtain differential interference contrast (DIC) images. Images were captured and processed with MetaMorph 7.1.2.0 (Molecular Devices, Downingtown, PA). Blind deconvolution was performed using a theoretical point spread function in Autoquant X2-64-bit software (Media Cybernetics, Bethesda, MD).

Tumor cell cytolysis assay

Tumor cells were seeded into a 96-well plate at a density of 10^4 cells per well and cultured overnight in DMEM. Neutrophils in DMEM were used at a concentration of 5×10^5 cells per well. Tumor cells were opsonized with anti-β2 microglobulin as described above. Tumor cells were labeled with Calcein-AM (Invitrogen) for 30 min at 37°C then washed thoroughly. Triplicate wells received the following treatments: DMEM (no treatment), neutrophils, or detergent [1% Triton-X 100 (Sigma) in DMEM], while IgG-opsonized tumor cells received DMEM, BAPTA-treated neutrophils, or neutrophils. Plates were incubated at 37°C for 4 h. After incubation, supernatants were centrifuged to remove particulates. Supernatants were transferred to a fresh 96-well plate then read on a FlexStation II (Molecular Devices) using an excitation of 494 nm and emission of 517 nm. Fluorescence intensities were averaged over triplicate wells, and then normalized using the appropriate control. Intensities were converted to percent maximal cytolysis, using the detergent-treated set as 100% cytolysis.

Cell labeling for Ca^{2+} experiments

Cells were incubated with 5.5 μM fura red, 2.6 μM fluo-4 and 2% pluronic-127 in PBS for 1 h at 37°C. After incubation, cells were washed with PBS, re-suspended in Ca^{2+} imaging buffer (150 mM NaCl, 4 mM KCl, 25 mM HEPES, 3 mM $CaCl_2$, 5 mM pyruvate, 10 mM glucose, and 1 mg/ml BSA, pH 7.9) and incubated for a further 30 min at 37°C, to purge excess dye. Cells were washed with imaging buffer before use. In experiments where the Ca^{2+} buffer BAPTA was used, cells were treated at a concentration of 10 μM BAPTA for 30 min at 37°C, then washed before use.

Super-quiet microfluorometry

Calcium signaling was detected with super-quiet microfluorometry using a previously described instrument [19]. Briefly, the illumination system utilizes a super-quiet mercury–xenon light source (Hamamatsu, Bridgewater, NJ) powered by a model 69907 arc lamp power supply (Newport Corp., Irvine, CA) and regulated by an Oriel light intensity controller (model 68950, Newport). Light was delivered to a Zeiss microscope via a liquid light guide attached to a custom Flash-Cube illumination device (Rapp OptoElectronic, Hamburg, Germany). The Flash-Cube diverted a fraction of the light to a cooled photodiode to provide a feedback signal for the light controller. Light was delivered to the sample using an HQ475/40× excitation filter and a 510 nm dichroic long-pass mirror (Chroma Technology Corp., Rockingham, VT). A D-104 microscope photometer [Photon Technology International (PTI), Birmingham, NJ], containing a 600 nm dichroic reflector, an HQ530/30m emission filter, and an HQ670/50m emission filter, was connected to two refrigerated PMT housings (Products for Research, Danvers, MA) each containing a Hamamatsu R1527P photon-counting photomultiplier tube. An adjustable diaphragm was used to exclude other cells from the measurements. Felix software (PTI) was used to analyze data. All experiments were performed in a dark room within an aluminum enclosure with the microscope stage set to 37°C.

Flashlamp imaging of Ca^{2+} microdomains

Neutrophils and tumor cells were placed on a 37°C heated stage in a cover-glass bottom dish at an effector-to-target ratio of 10:1. Excitation was provided by a Perkin-Elmer FX-4400 flashlamp, as described [20], which provided a

1 J/6 μs output. Samples were imaged at 10 frames/s using a Princeton Instruments PI-Max II intensified charge-coupled device detector attached to a Dual-View emission-splitting device (Optical Insights, Tuscon, AZ) that was, in turn, attached to a side port of a Nikon TE2000-U microscope. Samples were excited using an HQ475/40× filter and a 510 nm dichroic beamsplitter (Chroma). Emission light was directed into the Dual-View apparatus, which produces simultaneous images at two emission wavelengths. This utilized an HQ530/30m for fluo-4 emission, an HQ670/50 m for fura red emission, and a 600 nm dichroic reflector (Chroma). The result is an image stack wherein each frame is a dual image. WinSpec (dual image) files were imported into MetaMorph (Molecular Devices) where they were splitted and re-formatted. The files were opened in MetaFluor (Molecular Devices), where a ratio (fluo-4/fura red) image is produced. A threshold was applied to limit ratio calculations to within cell boundaries. A stepped color mask was applied to the ratio images, as visually illustrated (supplementary information, Fig. S1).

Results

Neutrophils exhibit Ca^{2+} signals during ADCC

In the first series of experiments, we tested the hypothesis that intracellular Ca^{2+} signals are elicited during neutrophil-to-tumor cell conjugate formation. Neutrophils were labeled with fluo-4 and fura red, which permit highly sensitive detection of Ca^{2+}-signaling events [19, 20]. Labeled neutrophils were added to IgG-opsonized tumor cells in cover-glass bottom culture dishes. Samples were scanned to identify leukocyte–tumor cell conjugates followed by super-quiet microfluorometric recording. In this method, illumination and detector noise are largely eliminated from the measurement, making a sample's quantum noise the major source of error. Figure 1a, trace 1, shows a fluorescence recording of the fluo-4/fura red ratio of a neutrophil bound to an IgG-opsonized tumor cell. As these data indicate, the fluorescence ratio increases in an oscillatory manner for several minutes followed by stabilization at a high level, which we interpret as high intracellular Ca^{2+} concentrations. To confirm that this increase in the fluo-4/fura red ratio was due to Ca^{2+}, neutrophils were treated with the Ca^{2+} buffer BAPTA at 10 μM in imaging buffer. When neutrophils were labeled with BAPTA, no enhanced fluorescence ratio could be detected in a neutrophil-IgG-coated tumor cell conjugate (Fig. 1a, trace 2). To demonstrate that the Ca^{2+} signal was specific for Ab-coated tumor cells, experiments were performed with fluo-4/fura red-labeled neutrophils in the presence of unopsonized tumor cells. In these experiments, no increase in the fluo-4/fura red ratio was observed (Fig. 1b), thus demonstrating Ab dependence. Hence, intracellular Ca^{2+} levels rise within neutrophils during ADCC.

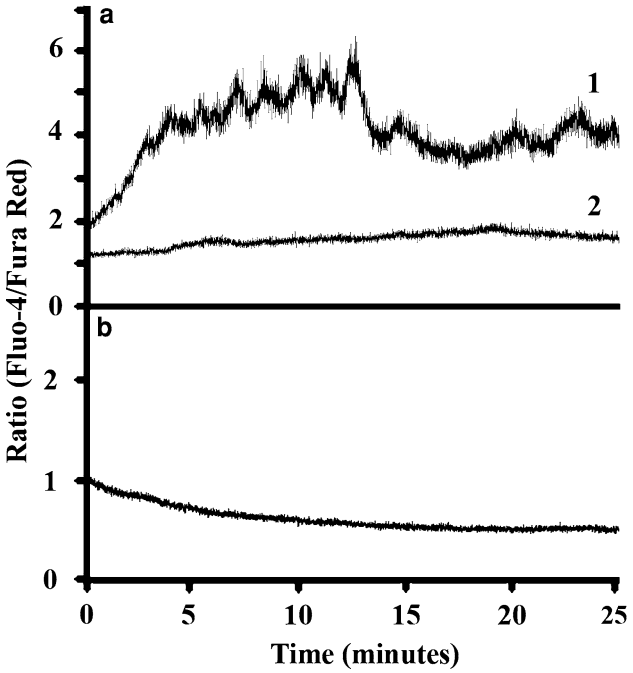

Fig. 1 Quantitative microfluorometry of Ca^{2+} signaling in single neutrophil–tumor cell conjugates. The fluo-4/fura red ratio is plotted at the ordinate and the time is given at the abscissa. All experiments were performed at 37°C using a highly stabilized microfluorometry system. In **a**, the *trace 1* shows a fluo-4/fura red-labeled neutrophil during incubation with an Ab-opsonized tumor cell. The fluo-4/fura red ratio oscillates in intensity as it increases in value, indicating a rise in intracellular Ca^{2+} concentration. Inclusion of the Ca^{2+} buffer BAPTA abrogated these changes, as indicated in the *trace 2* of **a**. As seen in **b**, no increase in the neutrophil's fluo-4/fura red ratio was observed when the tumor cells are not treated with opsonizing antibody ($n = 4$)

Ca^{2+} microdomains form at the neutrophil–tumor cell synapse

Although the microfluorometry studies above demonstrate that Ca^{2+} signals are associated with effector–target cell conjugates, they do not localize the Ca^{2+}-signaling sites within neutrophils. To localize Ca^{2+}-signaling sites within these cells, we used fluorescence image ratioing microscopy. We also used a flashlamp-based system for excitation to minimize the displacement of signals and probes by diffusion as well as movement of the cells and microdomains during image acquisition. Neutrophils were labeled with fluo-4 and fura red then incubated with IgG-opsonized tumor cell targets, as described in the preceding paragraph. Figure 2a and b shows a representative interaction between a neutrophil and a tumor cell over time. The DIC micrograph provides a lower magnification view of

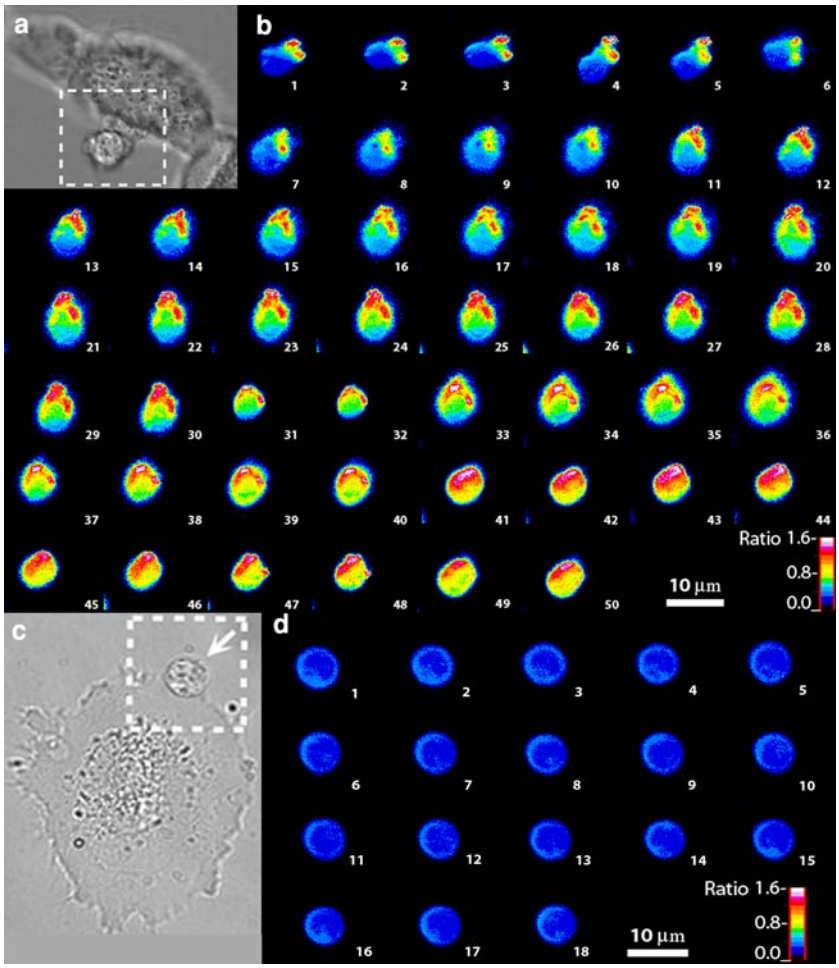

Fig. 2 Ca^{2+} microdomains are formed within neutrophils during ADCC. Neutrophils were labeled with fluo-4 and fura red. Tumor cells were opsonized with IgG. DIC (**a**) and fluorescence ratio images (**b**) of a neutrophil–tumor cell conjugate are shown. **a** DIC micrograph showing the region of neutrophil-to-tumor cell binding. The *boxed area* represents the region imaged in **b**. A representative sequence of micrographs illustrating the temporal evolution of the fluo-4/fura red ratio within the neutrophil over 37 min is shown in **b**. A 6 µs flashlamp was employed [20] to obtain each frame (supplemental information, Fig. S1). Each image corresponds to the sum of 50 consecutive frames (a 5-s average), with 40 s between each image. A color look-up-table was used to identify the ratios (*lower right hand side*). Broadly, the fluo-4/fura red ratio increased over time. Microdomains expressing a high fluo-4/fura red ratio were observed throughout the experiment. These regions exhibited dynamic properties, such as growth, fission, and fusion over the course of these observations. These microdomains were localized to the interface between the neutrophil and tumor cell target. The focusing of Ca^{2+} signals at this site may facilitate the local activation of leukocyte effector functions, such as degranulation and oxidant production ($n = 11$). **c**, **d** Similar experiment except that the neutrophil was treated with BAPTA, as described above. The frames of **d** show that BAPTA prevents microdomain formation ($n = 6$) (*bar* 10 µm)

neutrophil and tumor cell locations. The fluorescence ratios at different time points are shown. The fluo-4/fura red ratio within neutrophils increases over time. Moreover, the Ca^{2+} signal is localized to the neutrophil–tumor cell synapse (Fig. 2a, b, animations 1–5), with much of the cell expressing low fluo-4/fura red ratios. Regions of high fluo-4/fura red ratios represent Ca^{2+} microdomains. As can be seen by examining Fig. 2a and b, these Ca^{2+} microdomains are not static: these membrane specializations undergo movement, growth, fusion, and fission over the course of the observations. To provide quantitative ratiometric data, images were examined using line profile analysis (supplementary information, Fig. S2). As these data show, the measured ratio is much higher at the neutrophil–tumor cell synapse. However, when neutrophils were treated with BAPTA as described above, no microdomains could be observed with image ratioing microscopy (Fig. 2c, d, animation 6). Moreover, in the absence of IgG, neutrophils did not display Ca^{2+} microdomains (animation 7). Hence, neutrophils are characterized by spatially and temporally varying Ca^{2+} signals during ADCC-mediated destruction of tumor cells.

Disposition of Ca^{2+} regulatory proteins

The mechanism promoting Ca^{2+} microdomain formation likely involves local activation of the Ca^{2+}-signaling apparatus. As FcγR signaling has been linked to CRAC activity and CRAC activity has been linked with STIM1 clustering near the plasma membrane [21], neutrophil–tumor cell conjugates were fixed then labeled with an anti-STIM1 mAb followed by conventional fluorescence microscopy. These experiments showed that STIM1 was enhanced in the region of the neutrophil adjacent to the tumor cell (Fig. 3a, b). Thus, signal transduction elements downstream from FcγR that promote Ca^{2+} signaling are observed in the same region where microdomains are formed. As controls, we examined the dispositions of Ca^{2+}-binding proteins. For example, local depletion of Ca^{2+}-binding proteins at the neutrophil–tumor cell synapse would remove competition between the binding proteins and the fluorescent Ca^{2+} probes, thereby potentially increasing the probes' measured ratio. We, therefore, examined the intracellular distribution of Ca^{2+}-binding proteins. The neutrophil's Ca^{2+}-binding proteins calbindin and parvalbumin were not depleted in the region near the site of tumor cell contact (Fig. 3c, f). As the Ca^{2+}-signaling machinery, including Ca^{2+} buffering proteins, is located in the region of tumor cell contact, we suggest that an active signaling process is responsible for the formation of Ca^{2+} microdomains, not a passive enhancement due to the differential trafficking of Ca^{2+}-binding proteins.

Ca^{2+}-dependent stimulation of apoptosis and cytolysis

To examine the relevance of the Ca^{2+} signals described above in tumor cell death, we assessed apoptotic signaling in tumor cells during ADCC or control conditions. As Ca^{2+} signaling may promote apoptosis, we examined the ability of unlabeled neutrophils to elicit Ca^{2+} signals within IgG-opsonized fluo-4- and fura red-labeled HT-1080 cells. As anticipated, BAPTA inhibited the fluo-4/fura red signals within tumor cells (supplementary information, Fig. S3). Three markers of apoptotic signaling within tumor cells were evaluated: activation of caspase-3 using the NucView™ 488 caspase-3 substrate, GAPDH translocation to the nucleus of apoptotic cells, and annexin V binding to the cell surface. Although the NucView™ 488 caspase-3 substrate is not fluorescent, upon cleavage it becomes highly fluorescent and is delivered to the nucleus. Figure 4a shows a tumor cell incubated for 30 min at 37°C not only in the presence of the NucView™ 488 caspase-3 substrate, but also in the absence of neutrophils. As these data show, no accumulation of fluorescence is observed in the absence of neutrophils. However, in the presence of neutrophils, intense fluorescence is observed within tumor cells

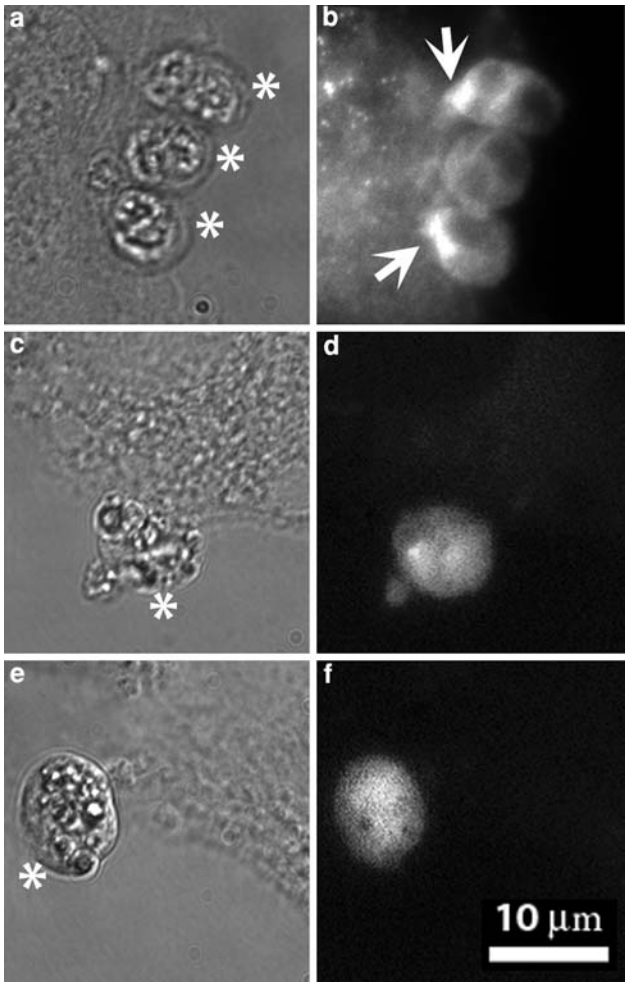

Fig. 3 Intracellular distribution of calcium regulatory proteins. Opsonized tumor cells were incubated in the presence of neutrophils. Differential interference contrast (*DIC*; **a**, **c** and **e**) images of neutrophil-bound HT-1080 cells and their corresponding fluorescence images (**b**, **d** and **f**) are shown. STIM1, calbindin, and parvalbumin were labeled using indirect immunofluorescence as described in "Materials and methods". Representative fluorescence micrographs of fixed and stained cells were acquired at room temperature using an EMCCD camera. STIM1 images were acquired for 200 ms. Calbindin and parvalbumin images used an exposure time of 2 s. STIM1 labeling was localized to the cellular region nearest the tumor cell (**a**, **b**, *arrows*). In contrast, calbindin (**c**, **d**) and parvalbumin (**e**, **f**) were found throughout the neutrophils. Hence, the Ca^{2+}-signaling element STIM1 accumulates at the neutrophil–tumor cell synapse whereas the Ca^{2+} buffering proteins calbindin and parvalbumin do not (*, neutrophil) (*bar* 10 µm) ($n = 4$)

(Fig. 4b), indicating the activation of caspase-3. When neutrophils were treated with BAPTA (Fig. 4c) or IgG, opsonization was omitted (Table 1), caspase-3 activation was not observed. A positive control experiment utilizing H_2O_2 exposure to promote apoptosis also exhibited caspase-3 activation (Fig. 4d). Quantitative data for all experiments are provided in Table 1. These findings indicate that apoptotic pathways within tumor cells are activated in the presence of neutrophils in an IgG- and Ca^{2+}-dependent fashion.

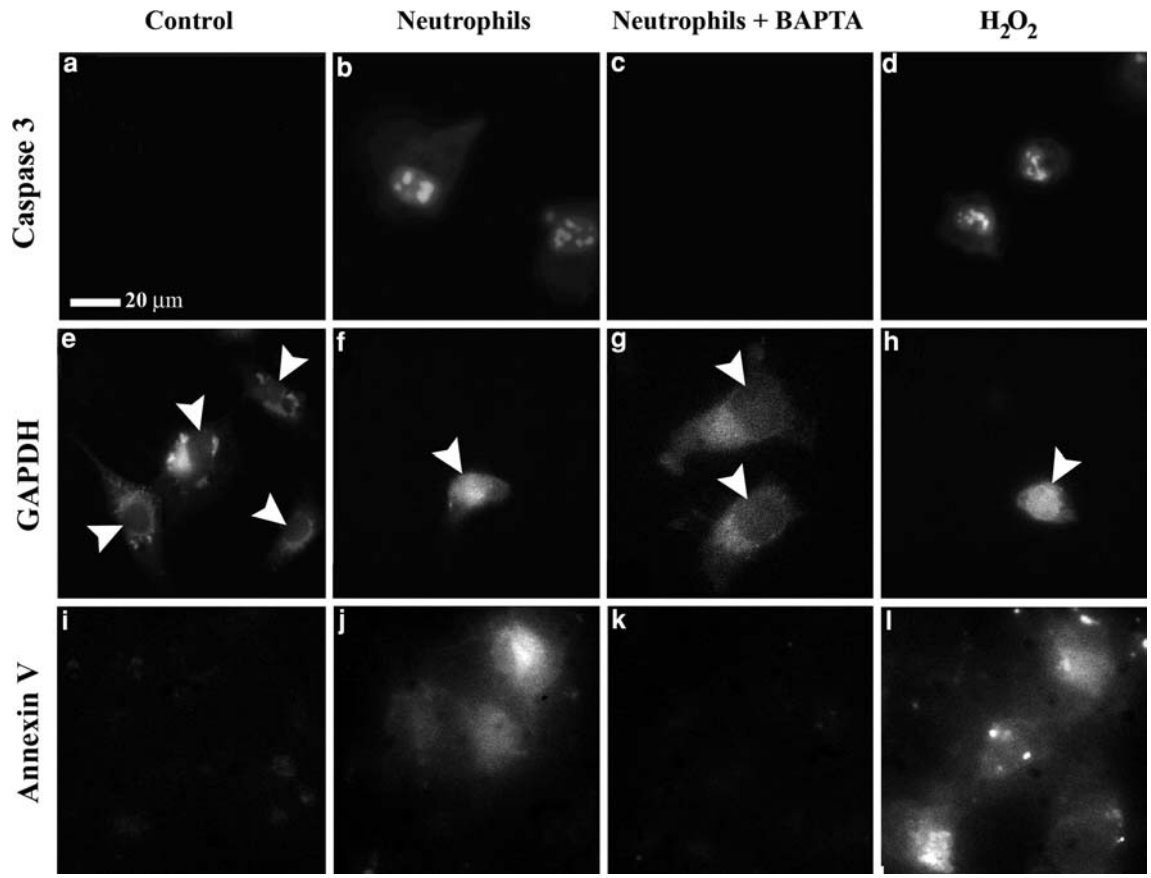

Fig. 4 ADCC is accompanied by apoptosis of tumor cells. Apoptosis was detected using caspase-3 activation, GAPDH translocation, and annexin V-binding assays. Opsonized tumor cells were incubated with the NucView™ 488 caspase-3 substrate for 30 min after incubation for 30 min in the absence or presence of neutrophils (**a**–**d**). **a** Control tumor cells incubated without neutrophils. No significant level of substrate fluorescence was observed. However, in the presence of neutrophils (**b**), intense fluorescence was observed indicating the activation of tumor cell caspase-3. Caspase-3 activation is dependent on Ca^{2+}, as indicated by neutrophils labeled with BAPTA (**c**). Positive controls using H_2O_2 show caspase-3 activation (**d**). Apoptosis was also examined using GAPDH translocation. In these studies opsonized tumor cells were incubated in the absence and presence of neutrophils for 4 h at 37°C. Samples were then fluorescently labeled with anti-GAPDH antibody using indirect immunofluorescence. Tumor cell nuclei are indicated with *arrowheads* in GAPDH (**e**–**h**). As shown in **e**, GAPDH is found in the cytoplasm of tumor cells, primarily as small clumps of fluorescence. However, when tumor cells are incubated with neutrophils, the fluorescence was primarily found within the nucleus (**f**). When tumor cells were treated with neutrophils labeled with the Ca^{2+} buffer BAPTA, GAPDH translocation was not observed (**g**). On the other hand, positive controls utilizing H_2O_2 exhibited GAPDH translocation (**h**). To test another apoptosis marker, annexin V binding was assessed (**i**–**l**). Opsonized tumor cells were incubated for 3 h in the presence or absence of neutrophils. Incubation with neutrophils results in high levels of annexin V binding (**j**), similar to that seen in the H_2O_2-stimulated positive control (**l**). The level of annexin V binding is reduced near the level of the negative control (**i**), when the neutrophils were treated with the Ca^{2+} buffer BAPTA (**k**). Quantitative data for the cell populations are shown in Table 1 (*bar* 20 μm)

Table 1 Quantitative summary of tumor cell apoptotic marker activation (n = 3–6)

Apoptotic marker	Treatments					
	Blank	Blank + IgG	Neutrophil	Neutrophil + IgG	Neutrophil + IgG + BAPTA	H_2O_2
Caspase-3	16.1 ± 4.9	17.8 ± 4.5	21.9 ± 11.0	68.6 ± 19.2[†]	15.0 ± 6.0	84.4 ± 11.9[‡]
GAPDH	21.2 ± 3.5	10.9 ± 1.6	16.1 ± 6.1	81.0 ± 11.0[‡]	32.1 ± 11.9	89.5 ± 12.2[‡]
Annexin V	10.1 ± 5.5	6.27 ± 4.8	20.2 ± 8.7	48.2 ± 9.2[‡]	17.5 ± 11.9	48.6 ± 9.5[‡]

[†] $P < 0.01$ in comparison to controls

[‡] $P < 0.001$ in comparison to controls

To provide another means of testing the activation of apoptotic signaling pathways, we examined GAPDH translocation to the tumor cell's nucleus. A recent study has shown that GAPDH translocation to the nucleus of neuronal cells is a biomarker of apoptotic activation [19]. We incubated opsonized tumor cells in the presence or absence of neutrophils for 4 h at 37°C. As glycolytic enzymes are frequently found to be associated with microfilaments or microtubules, which are highly sensitive to chemical fixation, samples were fixed using the DSP procedure described above; this highly permeable reagent rapidly fixes cells to retain their delicate internal structures. Samples were then labeled with anti-GAPDH Abs using indirect immunofluorescence. Figure 4e and f shows tumor cells incubated in the absence and presence of neutrophils, respectively. By comparing these micrographs, it is easy to see that the intracellular distribution of GAPDH varies greatly. In the absence of neutrophils, GAPDH is found in clusters throughout the cell cytoplasm, but is largely excluded from the nucleus. In contrast, cell samples incubated with neutrophils show GAPDH accumulation within the nucleus. This GAPDH translocation event was observed in a large proportion of cells, as indicated in Table 1. Furthermore, GAPDH accumulation in the nucleus was dependent on Ca^{2+} signaling, as suggested by experiments utilizing neutrophils treated with BAPTA (Fig. 4g). GAPDH translocation also required target opsonization (Table 1). Positive control experiments utilizing H_2O_2 to promote apoptosis also demonstrated GAPDH accumulation in the nucleus (Fig. 4h).

Annexin V binding is another well-established method to detect apoptotic cells. We conducted an assay in which opsonized tumor cells were incubated in the presence or absence of neutrophils for 3 h at 37°C. Cells were then treated with 5 µl Alexa Fluor 555-conjugated annexin V in media for 15 min at room temperature. After treatment, cells were washed and imaged. Figure 4j illustrates that neutrophil-treated tumor cells show bright annexin V labeling similar to that of the H_2O_2 stimulated positive control (Fig. 4l). As in previous assays, the apoptotic effect of the neutrophils appears to be reduced to near the level of the untreated control (Fig. 4i) when Ca^{2+} is buffered by treating neutrophils with BAPTA (Fig. 4k); this is further illustrated in quantitative data contained in Table 1. When Ab was omitted from tumor cell–neutrophil co-cultures, apoptosis was found at background levels (Table 1). As Alexa Fluor 350-conjugated annexin V absorbs in the ultraviolet, it was possible to triple label opsonized tumor cells with Fluo-4, Fura Red, and Alexa Fluor 350-conjugated annexin V. This experiment indicated that cells binding annexin V exhibit high Fluo-4/Fura Red ratios (supplemental information, Fig. S4). Hence, multiple assays indicate that neutrophils induce apoptosis during ADCC.

Finally, a tumor cell cytolysis assay showed that opsonized tumor cells treated with neutrophils for 3 h exhibited 37% (±16%) cytolysis relative to a detergent-treated control. As expected, the rate of cytolysis is dramatically lower than the acquisition of apoptotic markers in tumor cells (Table 1). However, treating the neutrophils with BAPTA reduced the measured extent of cytolysis to 15% (±11%). These several assays indicate that ADCC is taking place under the experimental conditions described above. Moreover, the formation of Ca^{2+} microdomains in neutrophils parallels the activation of apoptosis pathways in target cells.

Discussion

Ca^{2+} is a broadly important intracellular messenger that participates in numerous signaling events including leukocyte activation and tumor cell apoptosis [21, 23, 24]. In the present study, we examined the spatial and temporal properties of neutrophil Ca^{2+} signaling using the enhanced precision of super-quiet microfluorometry and flashlamp-based microscopy to illuminate the processes underlying ADCC. Using super-quiet microfluorometry, we have shown that Ca^{2+} signals increase in intensity and oscillate within neutrophils during ADCC. The comparatively long period of the oscillations is likely due to the imaging buffer. For example, the inclusion of pyruvate at a physiological concentration would be expected to lengthen the open time of Ca^{2+} channels [25]. Interestingly, during tumor cell killing, the noise associated with the Ca^{2+} signal was substantially greater than the expected quantum noise, suggesting that this represents chemical noise in the signal transduction apparatus [26]. Our studies in Fig. 2b provide strong evidence based on the fluo-4/fura red ratio that a steep Ca^{2+} gradient exists in neutrophils at the neutrophil–tumor cell interface during ADCC. Hence, a microdomain of high Ca^{2+} concentration forms in neutrophils at the neutrophil–tumor cell interface during ADCC.

The neutrophil–tumor cell synapse is a highly specialized region. The neutrophil plasma membrane receptors FcγRIIIb and FcγRIIa [27–31] may contribute to the effector responses described in this study. An early event in tumor cell destruction is the accumulation of FcRs at the neutrophil–tumor cell synapse. Previous studies have shown that FcRs cluster at the neutrophil-target binding site during ADCC [32]. Cross-linked FcRs trigger phosphorylation events and traffic to detergent-resistant membrane domains, which are likely lipid rafts [33]. Specifically, FcγRIIIb has been identified in lipid rafts [34]. Another key component of the neutrophil–tumor cell synapse is CD11b/CD18 [complement receptor type 3 (CR3), Mac-1, Mo-1], which participates in IgG-dependent cell activation

independently of its role in binding complement fragment iC3b [e.g., 35]. CD11b/CD18 plays a key role in ADCC [36, 37], which includes the formation of the neutrophil–tumor cell synapse. This, in turn, has been shown to be important in FcR-mediated host resistance to melanoma [38]. STIM1, an important element in the calcium signaling machinery, has been shown to redistribute and cluster in a lipid raft-dependent manner at junctions of the endoplasmic reticulum and the plasma membrane [39]. Indeed, as shown in Fig. 3, STIM1 accumulates within neutrophils at the neutrophil–tumor cell synapse during ADCC. Thus, STIM1 is likely to be important in (1) leukocytes mediating ADCC directed against tumor cell targets and (2) the locomotion of cancer cells [40]. Local activation of FcRs likely promotes Ca^{2+} signaling and the accumulation of additional elements of the Ca^{2+} signal transduction machinery, such as STIM1. As FcRs traffic to the neutrophil–tumor cell synapse and to lipid rafts, it is likely that the synapse is enriched in lipid rafts. We suggest that the Ca^{2+} microdomains illustrated in Fig. 2 are a functional signaling analog of the structurally defined lipid rafts [41].

It has been variously proposed that neutrophil effector functions such as degranulation and reactive oxygen metabolite production are important in neutrophil-mediated ADCC [3, 42, 43]. Our work supports this concept. Ca^{2+} signaling has been reported to play important roles in both neutrophil degranulation and NADPH oxidase activation [44, 45]. By focusing the neutrophil's Ca^{2+}-signaling apparatus at the site of tumor cell binding, the leukocyte's destructive potential will be selectively activated at this location—the point nearest the tumor cell. Our findings concerning neutrophil-mediated ADCC underscore the findings of Stockmeyer et al. [46], which suggested that apoptosis is induced in breast cancer cells at low effector–target ratios during ADCC by the release of neutrophil granules and other components, and provide new details regarding the underlying mechanism.

Recently, apoptosis has been recognized as an important mechanism of tumor cell death during ADCC, especially at low (and likely more physiologically relevant) effector-to-target ratios [46]. Caspase-3 activation is a gold standard of apoptotic signaling in cells [47]. It is the best-recognized marker of both early and later steps of the apoptosis. In the present study, we demonstrated caspase-3 activation during early neutrophil-mediated ADCC, which was also observed by the addition of hydrogen peroxide to tumor cells. Moreover, as the inclusion of BAPTA blocks this process, the rise in tumor cell Ca^{2+} noted during ADCC (supplemental information, Fig. S3) is required for the activation of caspase-3. Hence, the formation of Ca^{2+} microdomains in neutrophils leads to Ca^{2+}-dependent caspase-3 activation and apoptosis of tumor targets.

To provide additional evidence to support the induction of apoptotic signaling pathways during ADCC, we also tested tumor cells for the nuclear translocation of GAPDH. Although GAPDH is a glycolytic enzyme, it has several additional functions [48]. For example, Shashidharan et al. [49] and Dastoor and Dreyer [22] have demonstrated that GAPDH translocation to the nucleus is a marker of apoptosis mediated by oxidant stress in neural cells. In the present work, we demonstrated that GAPDH is extranuclear in untreated cells, but accumulates in the nucleus in hydrogen peroxide-treated cells or tumor cells during neutrophil-mediated ADCC. Our work confirms and extends these findings by demonstrating the nuclear translocation of GAPDH in tumor cells. To the best of our knowledge, GAPDH translocation to the nucleus has not been previously associated with ADCC or tumor cell biology.

Our work has significant implications for improving the immunotherapy of cancer. As traditional biochemical and rational drug design relies upon studies conducted outside the confines of living cells, it is becoming apparent that live cell imaging has an important place in drug development [50]. As our studies suggest that Ca^{2+} microdomains are associated with tumor cell apoptosis, the screening of drugs could be based on Ca^{2+}-signaling patterns. For example, one could search for compounds that stimulate Ca^{2+} microdomains matching those described above to enhance cytotoxicity. One interesting potential target in ADCC is ceramide kinase products [51], which might be useful in enhancing store-operated channel activity of leukocytes.

Ab-based pharmaceuticals are being increasingly used in cancer immunotherapy [1]. In many cases, these mAbs are used in combined therapy protocols with cytotoxic drugs. Recently, there has been renewed interest in the Warburg effect and metabolically active drugs [52], such as dichloroacetate and other pyruvate dehydrogenase kinase inhibitors affecting lactic acidosis [53]. These drugs promote apoptosis in tumor cells by increasing carbon flux into the citric acid cycle and electron transport. In contrast, as shown by the data of others [46] and Figs. 3 and 4, ADCC induces apoptosis via signaling pathways that likely include Ca^{2+} signals and reactive oxygen metabolites. As ADCC and metabolic therapy promote apoptosis via different routes, it seems likely that a combined metabolic-immunotherapy approach would enhance the efficacy of the mAb treatment. Moreover, a local reduction in lactate production would increase local pH and, consequently, enhance effector function [54] and Ca^{2+} signaling [55]. Such an approach may also reduce the high costs associated with mAb therapy. We are now exploring the potential of both Ca^{2+}-active agents and pyruvate dehydrogenase kinase inhibitors to augment tumor cell apoptosis during ADCC.

Acknowledgments This work was supported by the NCI and by the Wilson Medical Foundation.

References

1. Adams GP, Weiner LM (2005) Monoclonal antibody therapy of cancer. Nat Biotechnol 23(9):1147–1157
2. Vokes EE, Chu E (2006) Anti-EGFR therapies: clinical experience in colorectal, lung, and head and neck cancers. Oncology 20(5 Suppl 2):15–25
3. Di Carlo E, Forni G, Lollini PL, Colombo MP, Modesti A, Musiani P (2001) The intriguing role of polymorphonuclear neutrophils in antitumor reactions. Blood 97(2):339–345
4. Desjarlais JR, Lazar GA, Zhukovsky EA, Chu SY (2007) Optimizing engagement of the immune system by anti-tumor antibodies: an engineer's perspective. Drug Discov Today 12(21–22):898–910
5. Hara I, Takechi Y, Houghton AN (1995) Implicating a role for immune recognition of self in tumor rejection: passive immunization against the brown locus protein. J Exp Med 182(5):1609–1614
6. Naftzger C, Takechi Y, Kohda H, Hara I, Vijayasaradhi S, Houghton AN (1996) Immune response to a differentiation antigen induced by altered antigen: a study of tumor rejection and autoimmunity. Proc Natl Acad Sci USA 93(25):14809–14814
7. Clynes R, Takechi Y, Moroi Y, Houghton A, Ravetch JV (1998) Fc receptors are required in passive and active immunity to melanoma. Proc Natl Acad Sci USA 95(2):652–656
8. Clynes RA, Towers TL, Presta LG, Ravetch JV (2000) Inhibitory Fc receptors modulate in vivo cytoxicity against tumor targets. Nat Med 6(4):443–446
9. Bibeau F, Lopez-Crapez E, Di Fiore F et al (2009) Impact of FcγRIIa-FcγRIIIa polymorphisms and KRAS mutations on the clinical outcome of patients with metastatic colorectal cancer treated with cetuximab plus irinotecan. J Clin Oncol 27(7):1122–1129
10. Cartron G, Dacheux L, Salles G et al (2002) Therapeutic activity of humanized anti-CD20 monoclonal antibody and polymorphism in IgG Fc receptor FcγRIIIa gene. Blood 99(3):754–758
11. Musolino A, Naldi N, Bortesi B et al (2008) Immunoglobulin G fragment C receptor polymorphisms and clinical efficacy of trastuzumab-based therapy in patients with HER-2/neu-positive metastatic breast cancer. J Clin Oncol 26(11):1789–1796
12. van de Winkel JGJ, Hogarth PM (1998) The immunoglobulin receptors and their physiological and pathological roles in immunity. Kluwer Academic Publishers, Dordrecht
13. Stadick H, Stockmeyer B, Kühn R et al (2002) Epidermal growth factor receptor and g250: useful target antigens for antibody mediated cellular cytotoxicity against renal cell carcinoma? J Urol 167(2 Pt 1):707–712
14. Stockmeyer B, Valerius T, Repp R et al (1997) Preclinical studies with FcγR bispecific antibodies and granulocyte colony-stimulating factor-primed neutrophils as effector cells against HER-2/neu overexpressing breast cancer. Cancer Res 57(4):696–701
15. Würflein D, Dechant M, Stockmeyer B et al (1998) Evaluating antibodies for their capacity to induce cell-mediated lysis of malignant B cells. Cancer Res 58(14):3051–3058
16. Challacombe JM, Suhrbier A, Parsons PG et al (2006) Neutrophils are a key component of the antitumor efficacy of topical chemotherapy with ingenol-3-angelate. J Immunol 177(11):8123–8132
17. Santana C, Noris G, Espinoza B, Ortega E (1996) Protein tyrosine phosphorylation in leukocyte activation through receptors for IgG. J Leukoc Biol 60(4):433–440
18. Safiejko-Mroczka B, Bell PB Jr (1996) Bifunctional protein cross-linking reagents improve labeling of cytoskeletal proteins for qualitative and quantitative fluorescence microscopy. J Histochem Cytochem 44(6):641–656
19. Clark AJ, Petty HR (2007) Super-quiet microfluorometry: examples of tumor cell metabolic dynamics. In: Méndez-Vilas A, Díaz J (eds) Modern research and educational topics on microscopy. FORMATEX, Spain, pp 403–408
20. Clark AJ, Petty HR (2008) Observation of calcium microdomains at the uropod of living morphologically polarized human neutrophils using flashlamp-based fluorescence microscopy. Cytometry A 73(7):673–678
21. Feske S (2007) Calcium signalling in lymphocyte activation and disease. Nat Rev Immunol 7(9):690–702
22. Dastoor Z, Dreyer JL (2001) Potential role of nuclear translocation of glyceraldehyde-3-phosphate dehydrogenase in apoptosis and oxidative stress. J Cell Sci 114:1643–1653
23. van de Winkel JG, Tax WJ, Jacobs CW, Huizinga TW, Willems PH (1990) Cross-linking of both types of IgG Fc receptors, FcγRI and FcγRII, enhances intracellular free Ca^{2+} in the monocytic cell line U937. Scand J Immunol 31(3):315–325
24. Rizzuto R, Pinton P, Ferrari D et al (2003) Calcium and apoptosis: facts and hypotheses. Oncogene 22(53):8619–8627
25. Bakowski D, Parekh AB (2007) Regulation of store-operated calcium channels by the intermediary metabolite pyruvic acid. Curr Biol 17(12):1076–1081
26. Melamed-Book N, Kachalsky SG, Kaiserman I, Rahamimoff R (1999) Neuronal calcium sparks and intracellular calcium "noise". Proc Natl Acad Sci USA 96(26):15217–15221
27. van de Winkel JG, Anderson CL (1991) Biology of human immunoglobulin G Fc receptors. J Leukoc Biol 49(5):511–524
28. van de Winkel JG, van Duijnhoven HL, van Ommen R, Capel PJ, Tax WJ (1988) Selective modulation of two human monocyte Fc receptors for IgG by immobilized immune complexes. J Immunol 140(10):3515–3521
29. Kávai M, Gyimesi E, Szücs G, Szegedi G (1991) Binding and endocytosis of erythrocytes sensitized with rabbit IgG via Fc γ receptors of human monocytes. Immunology 74(4):657–660
30. Flesch BK, Vöge K, Henrichs T, Neppert J (2001) Fcγ receptor-mediated immune phagocytosis depends on the class of FcγR and on the immunoglobulin-coated target cell. Vox Sang 81(2):128–133
31. Li P, Jiang N, Nagarajan S, Wohlhueter R, Selvaraj P, Zhu C (2007) Affinity and kinetic analysis of Fcγ receptor IIIa (CD16a) binding to IgG ligands. J Biol Chem 282(9):6210–6221
32. Petty HR, Francis JW, Anderson CL (1989) Cell surface distribution of Fc receptors II and III on living human neutrophils before and during antibody dependent cellular cytotoxicity. J Cell Physiol 141(3):598–605
33. Kwiatkowska K, Frey J, Sobota A (2003) Phosphorylation of FcγRIIA is required for the receptor-induced actin rearrangement and capping: the role of membrane rafts. J Cell Sci 116(Pt 3):537–550
34. David A, Fridlich R, Aviram I (2005) The presence of membrane Proteinase 3 in neutrophil lipid rafts and its colocalization with FcγRIIIb and cytochrome b558. Exp Cell Res 308(1):156–165
35. Petty HR, Worth RG, Todd RF (2002) Interactions of integrins with their partner proteins in leukocyte membranes. Immunol Res 25(1):75–95
36. van Spriel AB, Leusen JH, van Egmond M et al (2001) Mac-1 (CD11b/CD18) is essential for Fc receptor-mediated neutrophil cytotoxicity and immunologic synapse formation. Blood 97(8):2478–2486
37. Kushner BH, Cheung NK (1992) Absolute requirement of CD11/CD18 adhesion molecules, FcRII and the phosphatidylinositol-linked FcRIII for monoclonal antibody-mediated neutrophil anti-human tumor cytotoxicity. Blood 79(6):1484–1490

38. Van Spriel A, Van Ojik H, Bakker A et al (2003) Mac-1 (CD11b/CD18) is crucial for effective Fc receptor-mediated immunity to melanoma. Blood 101(1):253–258
39. Pani B, Ong H, Liu X et al (2008) Lipid rafts determine clustering of STIM1 in endoplasmic reticulum-plasma membrane junctions and regulation of store-operated Ca^{2+} entry (SOCE). J Biol Chem 283(25):17333–17340
40. Yang S, Zhang JJ, Huang XY (2009) Orai1 and STIM1 are critical for breast tumor cell migration and metastasis. Cancer Cell 15(2):124–134
41. Dykstra M, Cherukuri A, Sohn HW, Tzeng SJ, Pierce SK (2003) Location is everything: lipid rafts and immune cell signaling. Annu Rev Immunol 21:457–481
42. Dallegri F, Patrone F, Frumento G, Sacchetti C (1984) Antibody-dependent killing of tumor cells by polymorphonuclear leukocytes. Involvement of oxidative and nonoxidative mechanisms. J Natl Cancer Inst 73(2):331–339
43. Hafeman DG, Lucas ZJ (1979) Polymorphonuclear leukocyte-mediated, antibody-dependent, cellular cytotoxicity against tumor cells: dependence on oxygen and the respiratory burst. J Immunol 123(1):55–62
44. Borregaard N, Cowland JB (1997) Granules of the human neutrophilic polymorphonuclear leukocyte. Blood 89(10):3503–3521
45. Lew PD (1990) Receptors and intracellular signaling in human neutrophils. Am Rev Respir Dis 141(3 Pt 2):S127–S131
46. Stockmeyer B, Beyer T, Neuhuber W et al (2003) Polymorphonuclear granulocytes induce antibody-dependent apoptosis in human breast cancer cells. J Immunol 171(10):5124–5129
47. Mazumder S, Plesca D, Almasan A (2008) Caspase-3 activation is a critical determinant of genotoxic stress-induced apoptosis. Methods Mol Biol 414:13–21
48. Chuang DM, Hough C, Senatorov VV (2005) Glyceraldehyde-3-phosphate dehydrogenase, apoptosis, and neurodegenerative diseases. Annu Rev Pharmacol Toxicol 45:269–290
49. Shashidharan P, Chalmers-Redman RM, Carlile GW et al (1999) Nuclear translocation of GAPDH-GFP fusion protein during apoptosis. Neuroreport 10(5):1149–1153
50. Netterwald J (2008) Lights! Camera! Action!. Drug Discov Dev 11(2):18–22
51. Hinkovska-Galcheva V, Clark AJ, Hiraoka M et al (2007) Ceramide kinase mediates store operated calcium signals and enhances phagolysosomal fusion. J Lipid Res 49(3):531–542
52. Pan JG, Mak TW (2007) Metabolic targeting as an anticancer strategy: dawn of a new era? Sci STKE 2007(381):pe14
53. Bonnet S, Archer SL, Allalunis-Turner J et al (2007) A mitochondria-K+ channel axis is suppressed in cancer and its normalization promotes apoptosis and inhibits cancer growth. Cancer Cell 11(1):37–51
54. Lardner A (2001) The effects of extracellular pH on immune function. J Leukoc Biol 69(4):522–530
55. Zablocki K, Szczepanowska J, Duszynski J (2005) Extracellular pH modifies mitochondrial control of capacitative calcium entry in Jurkat cells. J Biol Chem 280(5):3516–3521